

Extemporaneous Mechanochemistry: Shockwave Induced Ultrafast Chemical Reactions Due to Intramolecular Strain Energy

Brenden W. Hamilton¹, Matthew P. Kroonblawd², Alejandro Strachan^{1*}

¹School of Materials Engineering and Birck Nanotechnology Center, Purdue University, West Lafayette, Indiana, 47907 USA

²Physical and Life Sciences Directorate, Lawrence Livermore National Laboratory, Livermore, California 94550, United States

Abstract

Regions of energy localization referred to as hotspots are known to govern shock initiation and the run-to-detonation in energetic materials. Mounting computational evidence points to accelerated chemistry in hotspots from large intramolecular strains induced via the interactions between the shockwave and microstructure. However, definite evidence mapping intramolecular strain to accelerated or altered chemical reactions has so far been elusive. From a large-scale reactive molecular dynamics simulation of the energetic material TATB, we map molecular temperature and intramolecular strain energy prior to reaction to decomposition kinetics. Both temperature and intramolecular strain are shown to accelerate chemical kinetics. A detailed analysis of the atomistic trajectory shows that intramolecular strain can induce a mechanochemical alteration of decomposition mechanisms. The results in this paper can inform continuum-level chemistry models to account for a wide range of mechanochemical effects.

* strachan@purdue.edu

Shock loading can rapidly initiate numerous phenomena such as phase transitions^{1,2} and chemistry³⁻⁵, as well as plasticity, fracture, and failure^{6,7}. While these processes are also observed under static and slower loading rates⁸⁻¹¹, the ultrafast loading and transient states induced by a shockwave can result in exotic processes such as virtual melting^{12,13}, metallization of molecular crystals^{14,15}, and mechanochemistry¹⁶⁻¹⁸. A growing body of evidence suggests that ultrafast non-equilibrium processes can play a significant role in the initiation of high explosives (HEs).

The initiation of chemical reactions and transition to detonation in composite HE formulations under dynamical loading is dominated by energy localization into hotspots via the interaction of the shockwave with the microstructure¹⁹. These hotspots are almost exclusively characterized by their temperature fields²⁰⁻²³. However, recent molecular dynamics (MD) simulations indicate a deviation from this traditional picture. Dynamical hotspots can be significantly more reactive than thermodynamically equivalent ones created under non-shock conditions.^{24,25} Path-dependent reactivity and mechanochemistry have been proposed to explain these observations. However, direct isolation of the underlying non-equilibrium mechanochemical processes and their effect on shock-induced chemistry remains elusive.

In the context of gas-phase chemistry, quantum chemistry²⁶ studies have revealed how individual molecules respond to external forces^{27,28} and can result in alternate or forbidden reaction pathways^{29,30}. Applications-oriented studies have revealed that mechanochemical processes can couple synergistically with environmental factors to accelerate polymer degradation^{31,32}, optimize industrial reactions^{33,34}, and attenuate shock waves^{35,36}.

Mechanochemistry has also been studied in condensed phases. Examples include pure carbon³⁷, polypeptides,³⁸ and HE crystals³⁹. These studies show a variety of non-thermal reaction acceleration mechanisms and the potential for altered reaction pathways that arise from deformation mechanisms that operate on multi-nanometer length scales well beyond that of the individual molecules. These state-of-the-art studies for condensed matter mechanochemistry deliberately introduce mechanical perturbations to affect chemistry. How possible mechanochemistry occurs spontaneously under realistic loading conditions and how the various chemical paths conspire to determine the global response of the system remain open questions.

Most of the above work has focused on how to activate and control mechanochemistry, henceforth denoted as “premeditated mechanochemistry”. These are cases in which the system or experiment is designed to undergo mechanochemical activation when triggered, for both basic sciences and engineering materials purposes, as the inherent premeditated nature of the event makes it easier to study and harness. We instead focus on the distribution of molecular scale responses originating from realistic dynamical loading conditions, i.e., “extemporaneous mechanochemistry”. Examples of this can include impacts of planetary bodies^{4,38,40}, detonation events in solid energetics^{15,16}, and shearing of materials in earth’s core and between tectonic plates^{37,41}. The key to understanding extemporaneous mechanochemistry is not just the trends, but to map the physical chemistry processes involved to understand the overall governing dynamics of mechanochemistry. Here, we aim to study the entire extemporaneous event via the shock initiation of a porous sample of TATB (1,3,5-triamino-2,4,6-trinitrobenzene), an insensitive HE material. Our simulation set up is designed with inspiration from previous studies^{24,42,43} to provide the best opportunity to see an extemporaneous mechanochemical event.

Recent MD simulations revealed that the shock-induced collapse of porosity results not just in energy localization in the form of heating but also in significant intramolecular strains^{42,43}. The excess potential energy (PE), or intramolecular strain energy⁴⁴, is readily stored in modes relevant to prompt chemical initiation and exceeds the expected value based on the thermal vibrational

energy⁴². Similarly, quantum-chemistry calculations indicate that HOMO-LUMO gap closure arises in TATB when nitro groups are deformed out of plane, correlating mechanochemical effects with torsional (4-body) strains⁴⁵. We define the excess, or latent, PE for each molecule as the difference between the actual internal PE (U_{intra}) and that expected from equipartition of energy corresponding to the molecule's instantaneous temperature:

$$U_{latent} = [U_{intra} - U_0] - \frac{3N - 6}{2} k_b (T - 300)$$

where U_{intra} is determined from a single point calculation of each individual molecule only considering internal interactions, U_0 is the average U_{intra} in a 300 K perfect crystal, N is the number of atoms in the molecule, and T is the roto-vibrational kinetic energy of the molecule in units of kelvin. Additionally, we also quantified the strain energy originating from the ReaxFF four-body terms⁴⁶ (torsional and improper dihedrals) which will be referred to as U_{4-body} .

We performed large-scale, *reactive* MD simulations to characterize the effect of the latent energy in hotspots to induce extemporaneous mechanochemistry. Using a cylindrical pore of 40nm in diameter, we focus on relatively strong shocks where the resulting hotspots can transition to a deflagration wave within 10s of picoseconds^{24,47}. Figure 1 shows the evolution of temperature and U_{4-body} in the central hotspot, radiating shear bands, and surrounding material. Directly after pore collapse, both values rise significantly within the hotspot area. Following this initial formation stage, the high temperature region grows as the hotspot transitions towards a deflagration and the reaction zone expands driven by exothermic reactions. In contrast, the U_{4-body} term begins to relax within a few picoseconds of the collapse. This is driven by chemical reactions, which alleviate molecular strain on the 4-body terms measured here. Additionally, regions that react without significant molecular strain will also tend towards U_{4-body} values of zero as most gaseous products do not have four-body intramolecular components (CO_2 , H_2O , N_2 , etc.).

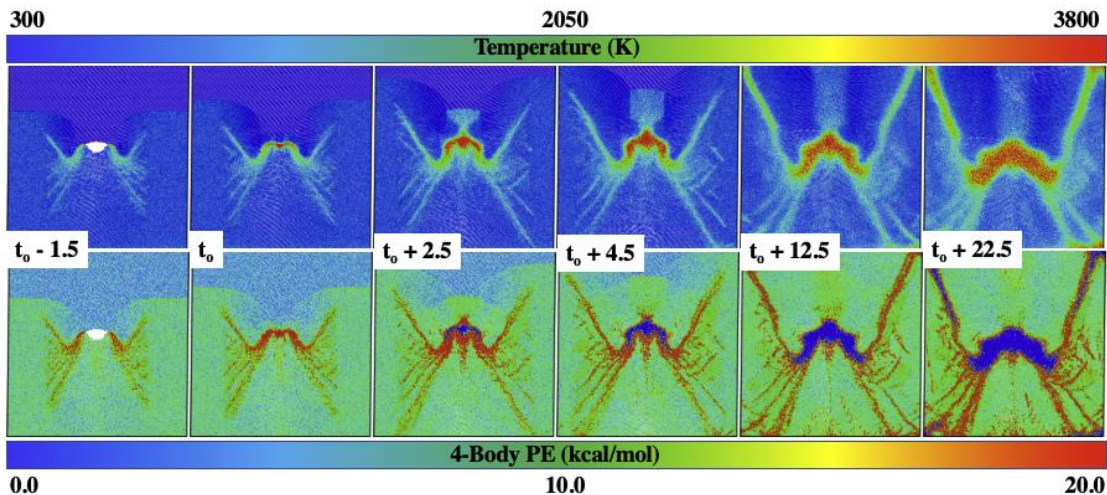


Figure 1: Time history of roto-vibrational temperature and 4-body PE in a reacting pore-collapse hot spot in TATB. The time origin t_0 corresponds to complete collapse of the pore, with time offsets given in picoseconds.

To characterize the role of U_{latent} on chemical kinetics we characterize the thermodynamic state of each molecule that fully reacts during the simulation time by computing its temperature and U_{Latent} right before reaction initiation, at time $t = t_1 - 0.1 \text{ ps}$. Here, t_1 is the initial decomposition time, defined as the first reaction in the molecule. To obtain a measure of total

reaction time, a second time (t_2) is defined as the first C-C ring bond scission. We define reaction time as $\tau_{Rxn} = t_2 - t_1$. We cluster all reacting molecules by their U_{latent} and temperature using an unsupervised k-means cluster analysis, see Figure 2a. Figure 2b shows the resulting cluster centroids for 6 clusters, mapped in temperature-strain energy space. All points in Figure 2 are colored by their cluster's average τ_{Rxn} , also indicated as inset text. Supplemental Materials section SM-1 lists the coordinates and reaction times for the cluster centroids. While clustered molecules are localized in $T-U_{latent}$ space, molecules within a given cluster are spatially distributed about the hotspot (see Figure 2c).

From the cluster centroids, two distinct trends are clear. The first, which is anticipated from Arrhenius kinetics, is that increasing temperature leads to faster reactions. Clusters 1, 2, and 3 all have similar intramolecular strain energy and exhibit a systematic decrease in τ_{Rxn} with increasing temperature. The second trend, which is somewhat expected from premeditated mechanochemistry studies, is a decrease in τ_{Rxn} with an increase in U_{Latent} . Clusters 2, 4, and 5 have roughly the same average temperature and exhibit a reduction in reaction time with increasing strain. Note that Cluster 5 has a significantly lower τ_{Rxn} than Cluster 3, despite being 240 K colder than Cluster 3.

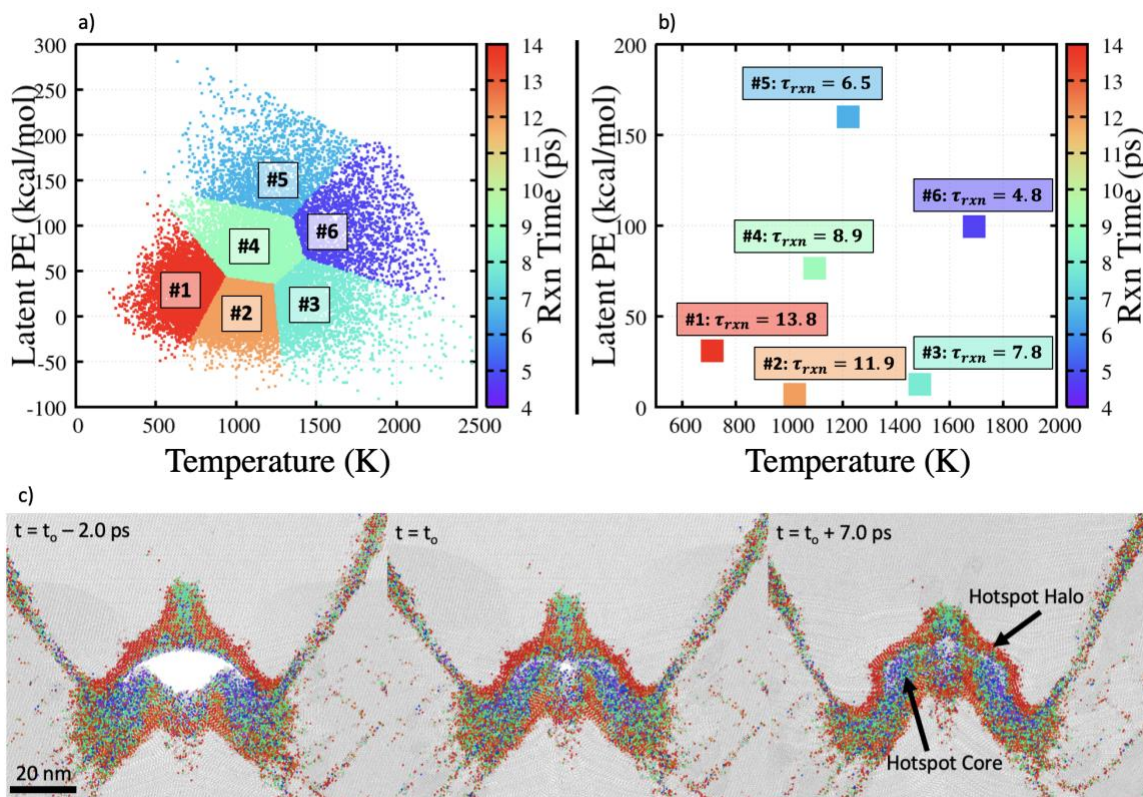


Figure 2: Molecular descriptors (a) and cluster centroids (b) colored by τ_{Rxn} plotted in $T-U_{latent}$ space. (c) Spatial mapping of clustered molecules about the hotspot during and after its formation. Molecules are colored by cluster ID following the convention in panels a and b, with non-clustered molecules colored white.

Spatial mapping of clustered molecules reveals several important trends. First, the slowest reacting clusters (i.e., 1 and 2) are mostly found in a “halo” around the “core” of the hotspot. In contrast, the hotspot core contains a mixture of molecules from the mechanochemically activated clusters (i.e., 4, 5, and 6) and the cluster of hot undeformed molecules (Cluster 3). This indicates that the accelerated reaction kinetics observed within hotspots determined from previous reactive MD simulations of pore collapse²⁴ is almost certainly mechanochemical in origin. There is also a

noticeable (but smaller) population of cluster 4, 5, and 6 molecules within the shear bands that emanate from the central hotspot, which is consistent with previous work¹⁷ showing accelerated reaction kinetics in shear bands. It is evident that the molecules with the largest U_{latent} are situated in regions exhibiting the greatest degree of plastic flow. This indicates that the acceleration of chemistry in hotspots and shear bands is fundamentally connected to deviatoric material response through mechanochemistry and is not simply a product of local variations in pressure or density, which are largely uniform across the hotspot.

Figure 3 depicts the underlying distributions of τ_{rxn} times for the Clusters 2, 3, and 5. In all cases, we observe the expected Maxwell-Boltzmann-like distributions, but the effect of U_{latent} is quite remarkable. Cluster 3 has a higher temperature than Cluster 2 and approximately the same U_{latent} , and as expected the reaction times are shorter. On the other hand, Cluster 5 has a similar temperature to Cluster 2, but with substantially higher U_{Latent} . This leads to almost the same effect as increasing temperature. While temperature and intramolecular strain energy are not uncorrelated (Pearson Correlation Coefficient: 0.46 ± 0.04 ; 95% confidence interval from bootstrapping), these distributions corroborate the trends in the cluster centroids that the U_{Latent} of the molecule is directly affecting the reaction timescales. Cluster 3 and Cluster 5 have nearly the same distribution, despite being tails in the two different descriptors showing that U_{Latent} is generally acting in a similar manner to the temperature, in terms of altering the overall kinetics and its statistics.

We note that the clustering analysis is based on an instantaneous measurement of molecular temperature and U_{Latent} just before t_1 , and these quantities vary during the time interval measured as τ_{Rxn} . Specifically, the relaxation of U_{4-body} with time shown in Figure 1 largely coincides with reactions that occur during the time interval between the first reaction at t_1 and proceeding up through ring breakage at time t_2 . The decrease of τ_{Rxn} , or more explicitly, the earlier C-C ring bond scission with respect to the first reaction, shows an inherent memory effect of the strain and temperature state at the point of first reaction. That is, after the strained bonds begin to break and reduce U_{4-body} , the downstream reactions are still affected by the energy state of the molecule at first reaction.

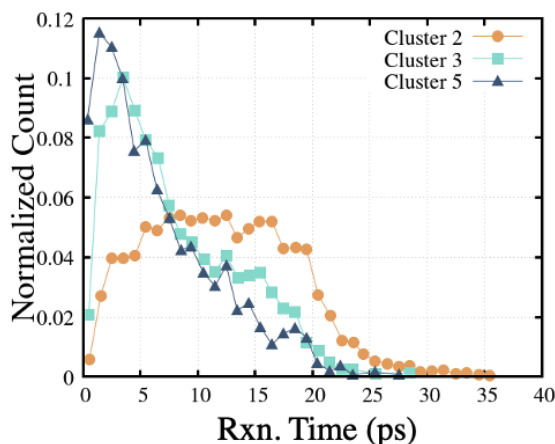


Figure 3: Distributions for τ_{Rxn} for Clusters 2, 3, and 5, which represent the hotspot average, high temperature tail, and high intramolecular strain tail, respectively.

Having established that multiple internal state variables of the decomposing molecule affect reaction kinetics, we now consider possible effects on decomposition paths. We focus on the first step of the decomposition of each molecule. Wu and Fried⁴⁸ showed that intramolecular hydrogen

transfer is the most likely first reaction for TATB. By comparison, intermolecular H transfer has an ~10 kcal/mol higher activation barrier than the uni-molecular reaction and NO₂ scission exhibits an even higher barrier than both H-transfers. Enhanced NO₂ scission has also been identified as a key difference for reactions in TATB shear bands compared to the bulk crystal¹⁷. Supplemental Materials section SM-2 shows schematics of these possible reactions. Here, chemical bonds are determined by ReaxFF bond tables with a 0.5 threshold⁴⁶.

By assessing the number of unimolecular and bimolecular hydrogen transfers, NO₂ scission, and ring fracture 1st step reactions in each cluster, we can track trends with increasing temperature and intramolecular strain energy, shown in Figure 4a and 4b. Methods used to determine reaction paths are described in Supplemental Materials section SM-3. Clusters 1, 2, and 3 show little to no intramolecular strain energy, with Cluster 3 being a high temperature, low strain tail. For the most part, these clusters show almost all common reactions, mainly the intramolecular hydrogen transfer, with Cluster 3 having about 25% intermolecular hydrogen transfer. Clusters 4 and 5, which have increasing U_{Latent} at similar average temperatures, show a few key trends. One is a large increase in the number of intermolecular hydrogen transfers, which ultimately make this route the dominant pathway, the other being an increase in the number of NO₂ scission reactions and a ring fracture events as the first step, albeit in trace amounts. (Note that this does not necessarily imply that these reactions are not common as downstream processes.) Cluster 6, which is a high temperature, mid-strain state, shows similar results to Cluster 5 with slightly lower counts for the “uncommon” first-step reactions. These agree well with previously reported premeditated TATB mechanochemistry¹⁸.

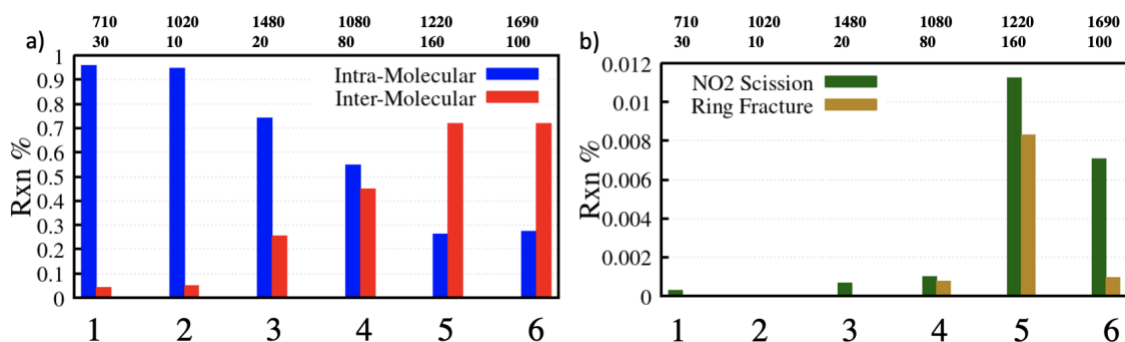


Figure 4: Bar charts of the percentages of first step reaction pathways for 4 reaction classes, organized by the cluster IDs presented in Figure 2 and split into groups of common (a) and uncommon (b) reactions.

Overall, we show through large-scale reactive MD simulations a significant acceleration and alteration of reactions in explosive hotspots due to local intramolecular strains that is not accounted for in “traditional” thermal chemistry models. This implies that HE shock initiation is fundamentally an extemporaneous mechanochemical process. A cluster analysis of the reacting molecules in our simulations links an acceleration of chemistry to increases in molecular temperature and U_{Latent} in which the mechanochemistry effect is localized to areas that undergo significant plastic flow. Additionally, U_{Latent} is found to alter the τ_{Rxn} distribution shape similar to temperature. An assessment of the first step reaction pathways for each cluster shows that increasing both temperature and U_{Latent} can lead to common, alternate reaction paths becoming dominant, and uncommon reaction paths appear in the high temperature and high U_{Latent} tails.

Our results show a direct relation between the level of intramolecular strain energy and reaction timescales, brought on in an extemporaneous manner. While these events occur at the level of

material microstructure, they involve a wide range of subscale molecular states and deformations that lead to a highly mixed, ensemble response. Upscaling these physics holds promise to improve the transferability of continuum-level explosive models^{17,42}, and of mechanochemical effects in a wide range of other functional molecular and polymeric materials^{31,32,34,35}. The connections between subscale molecular states and microstructural-level material dynamics revealed here indicate that a hybrid modeling approach may be best for rapidly screening for mechanochemical effects in other systems. This approach would combine large, yet efficient non-reactive simulations that explicitly resolve microstructural-level processes in atomic detail^{43,44} in tandem with small targeted reactive simulations¹⁸ that match distributions of U_{Latent} states to accelerate the exploration chemical phase space governing extemporaneous mechanochemical events.

Methods

Reactive, all-atom MD simulations were conducted using the ReaxFF forcefield⁴⁹ and the LAMMPS code⁵⁰. We use the so-called ReaxFF 2018⁵¹ parametrization, which has been used in past for TATB^{52,53} and is known to correctly predict first step reaction pathways^{48,53} and Hugoniot curves.⁵² Trajectories were integrated using a 0.1 fs time step. Partial atomic charges were calculated using the charge equilibration scheme⁵⁴ at each time step with an accuracy threshold set to 1×10^{-6} .

The simulation cell was built using the triclinic $P\bar{1}$ crystal structure⁵⁵ with equilibrium lattice parameters determined with ReaxFF 2018 at (300 K, 1 atm). We used an orthorhombic representation of the triclinic cell previously reported in Ref. ⁵² that was obtained using the generalized crystal cutting method⁵⁶. The orthorhombic cell was replicated to be ~250 nm in the shock direction (**C** vector) and approximately 120 nm along cell vector **A**. The simulation cell is periodic in **A** and **B** and open in the shock direction. A cylindrical pore with a circular cross-section 40 nm in diameter was cut in the **A-C** plane at fractional coordinate (1/2, 1/3), yielding a system with a total of 8.6 million atoms. The system was thermalized over 50ps of isothermal-isochoric (NVT) dynamics at 300 K with a Langevin thermostat⁵⁷, re-initializing velocities following a Maxwell-Boltzmann distribution every 5 ps. The shock simulation was run using a reverse ballistic setup⁵⁸ with a particle velocity of 2.0 km/s with dynamics propagated using microcanonical (NVE) equations of motion.

Analysis of the trajectories was performed in a molecularly averaged, center of mass (COM) framework. Two primary molecular properties were considered: roto-vibrational kinetic energy and intramolecular strain energy. We refer to the first term as temperature and use units of kelvin for simplicity (using the classical specific heat of $\frac{69}{2}k_b$). The second term was defined above in Equation 1.

We defined a molecular, characteristic reaction timescale, $\tau_{Rxn} = t_2 - t_1$, based on two well-defined events in the molecule's reaction history. Bond scission was determined using ReaxFF bond orders. Time t_1 was defined as the first bond scission in the molecule. Time t_2 was defined as the first C-C (ring) bond scission. SM-4 shows snapshots of both t_1 and t_2 events. MD snapshots were saved and analyzed every 0.1 ps, and a bond break must be observed for three consecutive frames for it to be considered a reaction. We performed the same analysis for thermal decomposition simulations to obtain a benchmark for interpreting changes in energy, see SM-5.

Acknowledgements

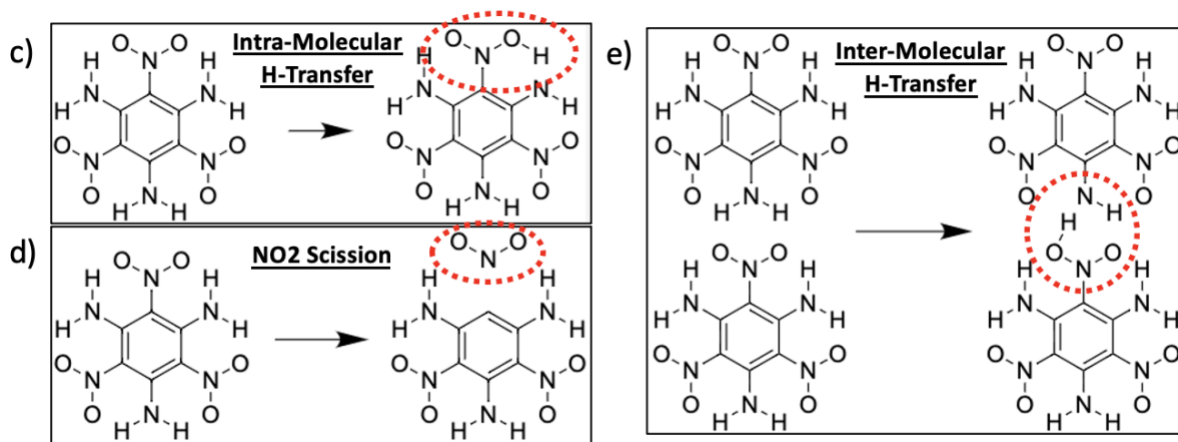
This work was supported by the Laboratory Directed Research and Development Program at Lawrence Livermore National Laboratory, project 18-SI-004 with Lara Leininger as P.I. Partial support was received from the US Office of Naval Research, Multidisciplinary University Research Initiatives (MURI) Program, Contract: N00014-16-1-2557. Program managers: Chad Stoltz and Kenny Lipkowitz. Partial support was received from the Army Research Laboratory and was accomplished under Cooperative Agreement Number W911NF-20-2-0189. Simulations were made possible by computing time granted to MPK through the LLNL Computing Grand Challenge, which is gratefully acknowledged. This work was performed under the auspices of the U.S. Department of Energy by Lawrence Livermore National Laboratory under Contract DE-AC52-07NA27344. It has been approved for unlimited release under document number LLNL-JRNL-834510-DRAFT.

SM-1: Cluster Centroids

SM Table 1: Cluster centroid data, as presented in Figure 2.

Cluster ID	Temperature (K)	U_{Latent} (kcal/mol)	τ_{Rxn} (ps)
1	710	30	13.8
2	1020	10	11.9
3	1480	20	7.8
4	1080	80	8.9
5	1220	160	6.5
6	1690	100	4.8

SM-2: Reaction Paths



SM- Figure 3: Schematics of the primary 1st step reaction paths for TATB.

SM-3: Chemical analysis details

ReaxFF simulations determine bonding on the fly via partial bond orders. From the bonding outputs, one can count the total number of bonds formed in a molecule, or with the atoms from an original molecule. For the 4 reactions tracked in this work, a distinction of reactions can be made by simply counting the bonds present. For each cluster, only trace amounts (1-2 molecules total) of reactions did not belong to one of the four reactions studied here.

We define as a molecular descriptor D the total bond counts B_i to atoms of each element type, which we track as a 4-dimensional vector $D = [B_C, B_H, B_N, B_O]$ for each molecule at each step throughout time. For instance, a C-O bond contributes +1 to B_C and +1 to B_O . This analysis only considers atom-atom connections and does not treat double and triple bonds differently than single bonds.

An unreacted TATB molecule has bonding [18, 6, 18, 6]. When a molecule does not match this pattern for 3 consecutive frames (0.3 ps), we take first frame of the three to be time t_1 .

Following t_1 , the patterns for identifying each reaction are as follows:

Intra-molecular hydrogen transfer: [18, 6, 18, <8]

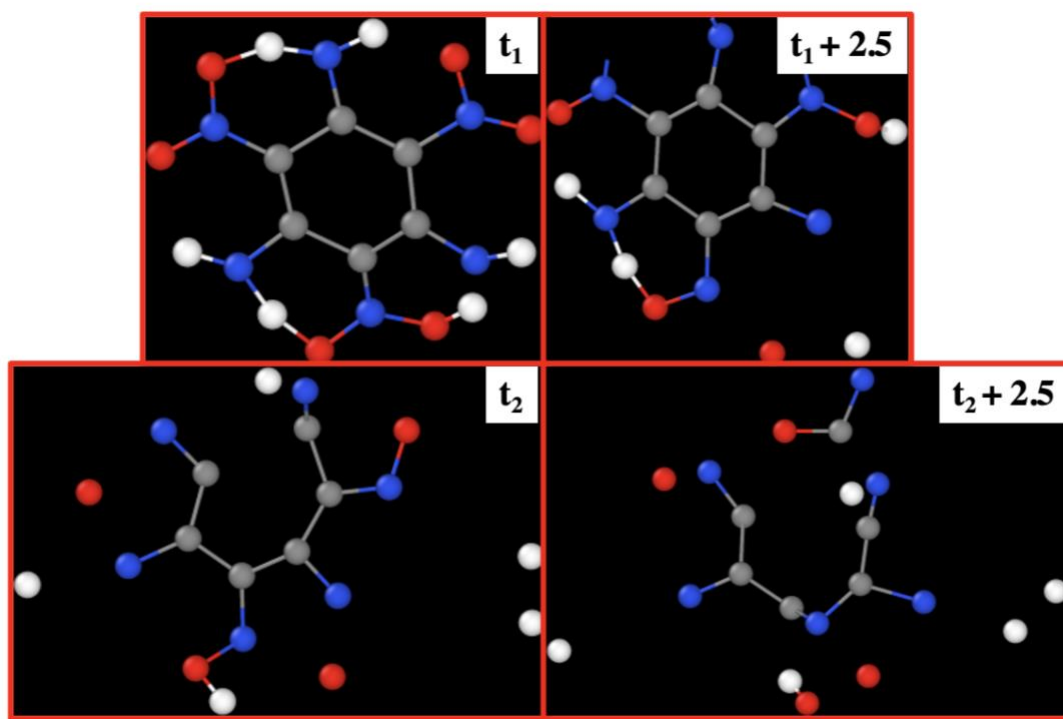
Inter-molecular hydrogen transfer: [18, 6, <18, 6]

NO₂ scission: [<18, 6, <18, 6]

Ring Fracture: [$<18, 6, 18, 6$]

SM-4: Example molecular structures at characteristic times

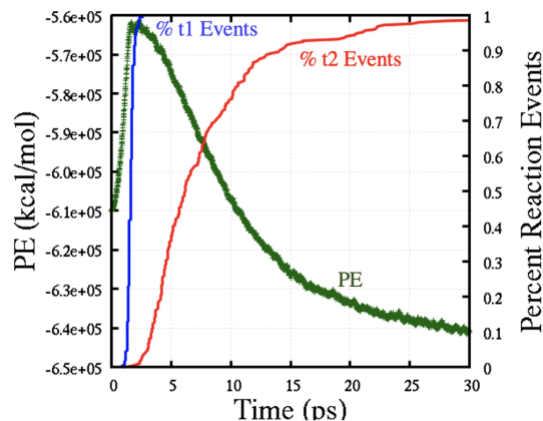
Example structures at times between t_1 and t_2 for an intra-molecular hydrogen transfer reaction.



SM Figure 1: Structures of a TATB molecule going through an intra-molecular hydrogen transfer reaction. Snapshots show an example molecule at the two characteristic times t_1 and t_2 defined in the main text, and at 2.5 ps after these times. Atoms are colored white, grey, blue, and red for H, C, N, and O.

SM-5: Time evolution of reactive events under isothermal conditions

We performed an isochoric-isothermal (NVT) decomposition simulation at 2500 K and ambient density to illustrate how t_1 and t_2 events evolve during the reaction as the total potential energy (PE) decays. The approach of cumulative t_1 events to unity corresponds to the completion of the 1st endothermic reaction step, and the approach of t_2 events to unity corresponds well to full exothermicity of the reaction.



SM Figure 2: PE time history and reaction events time history. Total system PE (green) corresponds to the left y axis, both reaction events (red and blue) correspond to the right y axis.

References

- (1) Kadau, K.; Germann, T. C.; Lomdahl, P. S.; Holian, B. L. Microscopic View of Structural Phase Transitions Induced by Shock Waves. *Science* (80-.). **2002**, *296* (5573), 1681–1684. <https://doi.org/10.1126/science.1070375>.
- (2) Kadau, K.; Germann, T. C.; Lomdahl, P. S.; Holian, B. L. Atomistic Simulations of Shock-Induced Transformations and Their Orientation Dependence in Bcc Fe Single Crystals. *Phys. Rev. B - Condens. Matter Mater. Phys.* **2005**, *72* (6), 1–14. <https://doi.org/10.1103/PhysRevB.72.064120>.
- (3) Strachan, A.; van Duin, A. C. T.; Chakraborty, D.; Dasgupta, S.; Goddard, W. A. Shock Waves in High-Energy Materials: The Initial Chemical Events in Nitramine RDX. *Phys. Rev. Lett.* **2003**, *91* (9), 7–10. <https://doi.org/10.1103/PhysRevLett.91.098301>.
- (4) Goldman, N.; Reed, E. J.; Fried, L. E.; William Kuo, I. F.; Maiti, A. Synthesis of Glycine-Containing Complexes in Impacts of Comets on Early Earth. *Nat. Chem.* **2010**, *2* (11), 949–954. <https://doi.org/10.1038/nchem.827>.
- (5) Armstrong, M. R.; Lindsey, R. K.; Goldman, N.; Nielsen, M. H.; Stavrou, E.; Fried, L. E.; Zaug, J. M.; Bastea, S. Ultrafast Shock Synthesis of Nanocarbon from a Liquid Precursor. *Nat. Commun.* **2020**, *11* (1), 1–7. <https://doi.org/10.1038/s41467-019-14034-z>.
- (6) Ravelo, R.; Germann, T. C.; Guerrero, O.; An, Q.; Holian, B. L. Shock-Induced Plasticity in Tantalum Single Crystals: Interatomic Potentials and Large-Scale Molecular-Dynamics Simulations. *Phys. Rev. B - Condens. Matter Mater. Phys.* **2013**, *88* (13), 1–17. <https://doi.org/10.1103/PhysRevB.88.134101>.
- (7) Bourne, N.; Millett, J.; Rosenberg, Z.; Murray, N. On the Shock Induced Failure of Brittle Solids. *J. Mech. Phys. Solids* **1998**, *46* (10), 1887–1908. [https://doi.org/10.1016/S0022-5096\(98\)00046-5](https://doi.org/10.1016/S0022-5096(98)00046-5).
- (8) Kroonblawd, M. P.; Lindsey, R. K.; Goldman, N. Synthesis of Functionalized Nitrogen-Containing Polycyclic Aromatic Hydrocarbons and Other Prebiotic Compounds in Impacting Glycine Solutions. *Chem. Sci.* **2019**, *10* (24), 6091–6098. <https://doi.org/10.1039/c9sc00155g>.
- (9) Strachan, A.; Lee Holian, B. Energy Exchange between Mesoparticles and Their Internal Degrees of Freedom. *Phys. Rev. Lett.* **2005**, *94* (1), 1–4. <https://doi.org/10.1103/PhysRevLett.94.014301>.
- (10) Lafourcade, P.; Denoual, C.; Maillet, J. B. Irreversible Deformation Mechanisms for 1,3,5-Triamino-2,4,6-Trinitrobenzene Single Crystal through Molecular Dynamics Simulations. *J. Phys. Chem. C* **2018**, *122* (26), 14954–14964. <https://doi.org/10.1021/acs.jpcc.8b02983>.
- (11) Zepeda-Ruiz, L. A.; Stukowski, A.; Ooppelstrup, T.; Bulatov, V. V. Probing the Limits of Metal Plasticity with Molecular Dynamics Simulations. *Nature* **2017**, *550* (7677), 492–495. <https://doi.org/10.1038/nature23472>.
- (12) Levitas, V. I.; Ravelo, R. Virtual Melting as a New Mechanism of Stress Relaxation under High Strain Rate Loading. *Proc. Natl. Acad. Sci. U. S. A.* **2012**, *109* (33), 13204–13207. <https://doi.org/10.1073/pnas.1203285109>.
- (13) Macatangay, J.; Hamilton, B. W.; Strachan, A. Deviatoric Stress Driven Transient Melting Below the Glass Transition Temperature in Shocked Polymers. *arXiv* **2022**.
- (14) Gilman, J. J. Shear-Induced Metallization. *Philos. Mag. B Phys. Condens. Matter; Stat. Mech. Electron. Opt. Magn. Prop.* **1993**, *67* (2), 207–214. <https://doi.org/10.1080/13642819308207868>.

- (15) Reed, E. J.; Manaa, M. R.; Fried, L. E.; Glaesemann, K. R.; Joannopoulos, J. D. A Transient Semimetallic Layer in Detonating Nitromethane. *Nat. Phys.* **2008**, *4* (1), 72–76. <https://doi.org/10.1038/nphys806>.
- (16) Eckhardt, C. J. Mechanochemistry: The Last Energetic Frontier. *Mol. Cryst. Liq. Cryst.* **2006**, *456* (1), 1–14. <https://doi.org/10.1080/15421400600786249>.
- (17) Kroonblawd, M. P.; Fried, L. E. High Explosive Ignition through Chemically Activated Nanoscale Shear Bands. *Phys. Rev. Lett.* **2020**, *124* (20), 206002. <https://doi.org/10.1103/PhysRevLett.124.206002>.
- (18) Hamilton, B. W.; Strachan, A. Many-Body Mechanochemistry : Intra-Molecular Strain in Condensed Matter Chemistry. *chemRxiv* **2022**.
- (19) Hamilton, B. W.; Sakano, M. N.; Li, C.; Strachan, A. Chemistry Under Shock Conditions. *Annu. Rev. Mater. Res.* **2021**, *51* (1), 101–130. <https://doi.org/10.1146/annurev-matsci-080819-120123>.
- (20) Li, C.; Hamilton, B. W.; Strachan, A. Hotspot Formation Due to Shock-Induced Pore Collapse in 1,3,5,7-Tetranitro-1,3,5,7-Tetrazoctane (HMX): Role of Pore Shape and Shock Strength in Collapse Mechanism and Temperature. *J. Appl. Phys.* **2020**, *127* (17). <https://doi.org/10.1063/5.0005872>.
- (21) Sakano, M. N.; Hamed, A.; Kober, E. M.; Grilli, N.; Hamilton, B. W.; Islam, M. M.; Koslowski, M.; Strachan, A. Unsupervised Learning-Based Multiscale Model of Thermochemistry in 1,3,5-Trinitro-1,3,5-Triazinane (RDX). *J. Phys. Chem. A* **2020**, *124* (44), 9141–9155. <https://doi.org/10.1021/acs.jpca.0c07320>.
- (22) Kroonblawd, M. P.; Hamilton, B. W.; Strachan, A. Fourier-like Thermal Relaxation of Nanoscale Explosive Hot Spots. *J. Phys. Chem. C* **2021**, *125*, 20570–20582. <https://doi.org/10.1021/acs.jpcc.1c05599>.
- (23) Sakano, M.; Hamilton, B. W.; Islam, M. M.; Strachan, A. Role of Molecular Disorder on the Reactivity of RDX. *J. Phys. Chem. C* **2018**, *122* (47), 27032–27043. <https://doi.org/10.1021/acs.jpcc.8b06509>.
- (24) Wood, M. A.; Cherukara, M. J.; Kober, E. M.; Strachan, A. Ultrafast Chemistry under Nonequilibrium Conditions and the Shock to Deflagration Transition at the Nanoscale. *J. Phys. Chem. C* **2015**, *119* (38), 22008–22015. <https://doi.org/10.1021/acs.jpcc.5b05362>.
- (25) Stavrou, E.; Bagge-Hansen, M.; Hammons, J. A.; Nielsen, M. H.; Steele, B. A.; Xiao, P.; Kroonblawd, M. P.; Nelms, M. D.; Shaw, W. L.; Bassett, W.; Bastea, S.; Lauderbach, L. M.; Hodgkin, R. L.; Perez-Martí, N. A.; Singh, S.; Das, P.; Li, Y.; Schuman, A.; Sinclair, N.; Fezzaa, K.; Deriy, A.; Leininger, L. D.; Willey, T. M. Detonation-Induced Transformation of Graphite to Hexagonal Diamond. *Phys. Rev. B* **2020**, *102* (10), 104116. <https://doi.org/10.1103/PhysRevB.102.104116>.
- (26) Stauch, T.; Dreuw, A. Advances in Quantum Mechanochemistry: Electronic Structure Methods and Force Analysis. *Chem. Rev.* **2016**, *116* (22), 14137–14180. <https://doi.org/10.1021/acs.chemrev.6b00458>.
- (27) Beyer, M. K. The Mechanical Strength of a Covalent Bond Calculated by Density Functional Theory. *J. Chem. Phys.* **2000**, *112* (17), 7307–7312. <https://doi.org/10.1063/1.481330>.
- (28) Ribas-Arino, J.; Marx, D. Covalent Mechanochemistry: Theoretical Concepts and Computational Tools with Applications to Molecular Nanomechanics. *Chem. Rev.* **2012**, *112* (10), 5412–5487. <https://doi.org/10.1021/cr200399q>.
- (29) Wang, J.; Kouznetsova, T. B.; Niu, Z.; Ong, M. T.; Klukovich, H. M.; Rheingold, A. L.; Martínez, T. J.; Craig, S. L. Inducing and Quantifying Forbidden Reactivity with Single-Molecule Polymer Mechanochemistry. *Nat. Chem.* **2015**, *7* (4), 323–327. <https://doi.org/10.1038/nchem.2185>.
- (30) Ong, M. T.; Leiding, J.; Tao, H.; Virshup, A. M.; Martínez, T. J. First Principles Dynamics and Minimum Energy Pathways for Mechanochemical Ring Opening of Cyclobutene. *J. Am. Chem. Soc.* **2009**, *131* (18), 6377–6379. <https://doi.org/10.1021/ja8095834>.
- (31) Kroonblawd, M. P.; Goldman, N.; Lewicki, J. P. Anisotropic Hydrolysis Susceptibility in Deformed Polydimethylsiloxanes. *J. Phys. Chem. B* **2019**, *123* (37), 7926–7935. <https://doi.org/10.1021/acs.jpcc.9b07159>.
- (32) Lupton, E. M.; Achenbach, F.; Weis, J.; Bräuchle, C.; Frank, I. Modified Chemistry of Siloxanes under Tensile Stress: Interaction with Environment. *J. Phys. Chem. B* **2006**, *110* (30), 14557–14563. <https://doi.org/10.1021/jp0607059>.
- (33) Mack, J.; Shumba, M. Rate Enhancement of the Morita–Baylis–Hillman Reaction through Mechanochemistry. *Green Chem.* **2007**, *9* (4), 328–333. <https://doi.org/10.1039/b612983h>.
- (34) Han, G. F.; Li, F.; Chen, Z. W.; Coppex, C.; Kim, S. J.; Noh, H. J.; Fu, Z.; Lu, Y.; Singh, C. V.; Siahrostami, S.; Jiang, Q.; Baek, J. B. Mechanochemistry for Ammonia Synthesis under Mild Conditions. *Nat. Nanotechnol.* **2021**, *16* (3), 325–330. <https://doi.org/10.1038/s41565-020-00809-9>.
- (35) Zhou, X.; Miao, Y. R.; Shaw, W. L.; Suslick, K. S.; Dlott, D. D. Shock Wave Energy Absorption in Metal–Organic Framework. *J. Am. Chem. Soc.* **2019**, *141* (6), 2220–2223. <https://doi.org/10.1021/jacs.8b12905>.
- (36) Shaw, W. L.; Ren, Y.; Moore, J. S.; Dlott, D. D. Mechanochemistry for Shock Wave Energy Dissipation. *AIP Conf. Proc.* **2017**, *1793* (January). <https://doi.org/10.1063/1.4971484>.
- (37) Kroonblawd, M. P.; Goldman, N. Mechanochemical Formation of Heterogeneous Diamond Structures during Rapid Uniaxial Compression in Graphite. *Phys. Rev. B* **2018**, *97* (18), 1–9. <https://doi.org/10.1103/PhysRevB.97.184106>.
- (38) Steele, B. A.; Goldman, N.; Kuo, I. F. W.; Kroonblawd, M. P. Mechanochemical Synthesis of Glycine Oligomers in a Virtual Rotational Diamond Anvil Cell. *Chem. Sci.* **2020**, *11* (30), 7760–7771. <https://doi.org/10.1039/d0sc00755b>.
- (39) Guo, D.; An, Q.; Goddard, W. A.; Zybin, S. V.; Huang, F. Compressive Shear Reactive Molecular Dynamics Studies Indicating That Cocrystals of TNT/CL-20 Decrease Sensitivity. *J. Phys. Chem. C* **2014**, *118* (51), 30202–30208. <https://doi.org/10.1021/jp5093527>.
- (40) Goldman, N.; Tamblyn, I. Prebiotic Chemistry within a Simple Impacting Icy Mixture. *J. Phys. Chem. A* **2013**, *117* (24), 5124–5131. <https://doi.org/10.1021/jp402976n>.
- (41) Kraus, D.; Rivasio, A.; Gauthier, M.; Gericke, D. O.; Vorberger, J.; Frydrych, S.; Helfrich, J.; Fletcher, L. B.; Schaumann,

- G.; Nagler, B.; Barbrel, B.; Bachmann, B.; Gamboa, E. J.; Göde, S.; Granados, E.; Gregori, G.; Lee, H. J.; Neumayer, P.; Schumaker, W.; Döppner, T.; Falcone, R. W.; Glenzer, S. H.; Roth, M. Nanosecond Formation of Diamond and Lonsdaleite by Shock Compression of Graphite. *Nat. Commun.* **2016**, *7*, 1–6. <https://doi.org/10.1038/ncomms10970>.
- (42) Hamilton, B. W.; Kroonblawd, M. P.; Li, C.; Strachan, A. A Hotspot's Better Half: Non-Equilibrium Intra-Molecular Strain in Shock Physics. *J. Phys. Chem. Lett.* **2021**, *12* (11), 2756–2762. <https://doi.org/10.1021/acs.jpcclett.1c00233>.
- (43) Hamilton, B. W.; Kroonblawd, M. P.; Strachan, A. The Potential Energy Hotspot: Effects from Impact Velocity, Defect Geometry, and Crystallographic Orientation. *J. Phys. Chem. C* **2022**.
- (44) Kroonblawd, M. P.; Steele, B. A.; Nelms, M. D.; Fried, L. E.; Austin, R. A. Anisotropic Strength Behavior of Single-Crystal TATB. *Model. Simul. Mater. Sci. Eng.* **2021**, *30* (1), 014004.
- (45) Manaa, M. R. Shear-Induced Metallization of Triamino-Trinitrobenzene Crystals. *Appl. Phys. Lett.* **2003**, *83* (7), 1352–1354. <https://doi.org/10.1063/1.1603351>.
- (46) Senftle, T. P.; Hong, S.; Islam, M. M.; Kylasa, S. B.; Zheng, Y.; Shin, Y. K.; Junkermeier, C.; Engel-Herbert, R.; Janik, M. J.; Aktulga, H. M.; Verstraelen, T.; Grama, A.; Van Duin, A. C. T. The ReaxFF Reactive Force-Field: Development, Applications and Future Directions. *npj Comput. Mater.* **2016**, *2* (September 2015). <https://doi.org/10.1038/npjcompumats.2015.11>.
- (47) Shan, T. R.; Wixom, R. R.; Thompson, A. P. Extended Asymmetric Hot Region Formation Due to Shockwave Interactions Following Void Collapse in Shocked High Explosive. *Phys. Rev. B* **2016**, *94* (5). <https://doi.org/10.1103/PhysRevB.94.054308>.
- (48) Wu, C. J.; Fried, L. E. Ring Closure Mediated by Intramolecular Hydrogen Transfer in the Decomposition of a Push-Pull Nitroaromatic: TATB. *J. Phys. Chem. A* **2000**, *104* (27), 6447–6452. <https://doi.org/10.1021/jp001019r>.
- (49) Van Duin, A. C. T.; Dasgupta, S.; Lorant, F.; Goddard, W. A. ReaxFF: A Reactive Force Field for Hydrocarbons. *J. Phys. Chem. A* **2001**, *105* (41), 9396–9409. <https://doi.org/10.1021/jp004368u>.
- (50) Plimpton, S. Fast Parallel Algorithms for Short-Range Molecular Dynamics. *J. Comput. Phys.* **1995**, *117* (1), 1–19. <https://doi.org/10.1006/jcph.1995.1039>.
- (51) Wood, M. A.; Kittell, D. E.; Yarrington, C. D.; Thompson, A. P. Multiscale Modeling of Shock Wave Localization in Porous Energetic Material. *Phys. Rev. B* **2018**, *97* (1), 1–9. <https://doi.org/10.1103/PhysRevB.97.014109>.
- (52) Hamilton, B. W.; Kroonblawd, M. P.; Islam, M. M.; Strachan, A. Sensitivity of the Shock Initiation Threshold of 1,3,5-Triamino-2,4,6-Trinitrobenzene (TATB) to Nuclear Quantum Effects. *J. Phys. Chem. C* **2019**, *123* (36), 21969–21981. <https://doi.org/10.1021/acs.jpcc.9b05409>.
- (53) Hamilton, B. W.; Steele, B. A.; Sakano, M. N.; Kroonblawd, M. P.; Kuo, I. F. W.; Strachan, A. Predicted Reaction Mechanisms, Product Speciation, Kinetics, and Detonation Properties of the Insensitive Explosive 2,6-Diamino-3,5-Dinitropyrazine-1-Oxide (LLM-105). *J. Phys. Chem. A* **2021**, *125* (8), 1766–1777. <https://doi.org/10.1021/acs.jpca.0c10946>.
- (54) Rappé, A. K.; Goddard, W. A. Charge Equilibration for Molecular Dynamics Simulations. *J. Phys. Chem.* **1991**, *95* (8), 3358–3363. <https://doi.org/10.1021/j100161a070>.
- (55) Cady, H. H.; Larson, A. C. The Crystal Structure of 1,3,5-Triamino-2,4,6-Trinitrobenzene. *Acta Crystallogr.* **1965**, *18* (3), 485–496. <https://doi.org/10.1107/s0365110x6500107x>.
- (56) Kroonblawd, M. P.; Mathew, N.; Jiang, S.; Sewell, T. D. A Generalized Crystal-Cutting Method for Modeling Arbitrarily Oriented Crystals in 3D Periodic Simulation Cells with Applications to Crystal–Crystal Interfaces. *Comput. Phys. Commun.* **2016**, *207*, 232–242. <https://doi.org/10.1016/j.cpc.2016.07.007>.
- (57) Dunweg, B.; Paul, W. Brownian Dynamics Simulations without Gaussian Random Numbers. *Int. J. Mod. Phys. C* **1991**, *2* (3), 817–827.
- (58) Holian, B. L.; Straub, G. K. Molecular Dynamics of Shock Waves in Three-Dimensional Solids: Transition from Nonsteady to Steady Waves in Perfect Crystals and Implications for the Rankine-Hugoniot Conditions. *Phys. Rev. Lett.* **1979**, *43* (21), 1598–1600. <https://doi.org/10.1103/PhysRevLett.43.1598>.